Superexcited states of NO studied by angle-resolved electron-energy-loss spectroscopy

Jian-Min Sun,[1] Zhi-Ping Zhong,[2,*] Lin-Fan Zhu,[1] Wen-Bin Li,[1] Xiao-Jing Liu,[1] Zhen-Sheng Yuan,[1] and Ke-Zun Xu[1]
[1]*Hefei National Laboratory for Physical Sciences at Microscale, Laboratory of Bond-Selective Chemistry, Department of Modern Physics, University of Science and Technology of China, Hefei, Anhui, 230027, China*
[2]*Department of Physics, Graduate School of the Chinese Academy of Sciences, P. O. Box 3908, Beijing 100039, China*
(Received 16 January 2004; revised manuscript received 3 May 2004; published 19 July 2004)

Absolute double differential cross section spectra of NO below 135 eV have been determined by an angle-resolved electron-energy-loss spectrometer with an incident electron energy of 2500 eV and an energy resolution of 100 meV. Some features above the first ionization threshold, which are too weak to be observed in the photoabsorption spectrum, stand out at large scattering angles. The present measured features and those unassigned ones in the fluorescence spectra [Chem. Phys. **293**, 65 (2003)] are assigned based on the present experimental work and theoretical analysis. The energy levels of $4\sigma^{-1}(c^3\Pi)ns\sigma(n=3-5)$, $4\sigma^{-1}(B\ ^1\Pi)ns\sigma(n=3-5)$, a vibrational resolved doubly excited state, and the inner-valence transition $2\pi \leftarrow 3\sigma$ are determined. Meanwhile, the ionization threshold (22.1 eV) of $(4\sigma)^{-1}\ B\ ^1\Pi$ is estimated.

DOI: 10.1103/PhysRevA.70.012708 PACS number(s): 34.80.Gs, 33.70.Fd, 31.15.Ne

I. INTRODUCTION

The electron-atom and molecule collision process extensively exists in many fields such as plasma physics, chemistry, gaseous discharge, and laser system, so the investigations of differential cross sections (DCSs) of electron scattering are helpful to the development of these fields. In addition, the DCSs of atoms and molecules determined by inelastic electron scattering are useful in gaining insight into the details of the collision mechanism. The generalized oscillator strength density (GOSD) plays the central role in inelastic collisions of fast charged particles[1], and it is directly related with the overlap integration between the initial-state and excited-state wave functions as the following definition (in atomic units)[1]:

$$\frac{df(K,E)}{dE} = \sum_n \frac{E_n}{K^2} |\langle \Psi_n | \sum_{j=1}^{N} \exp(i\mathbf{K}\cdot\mathbf{r}_j) | \Psi_0 \rangle|^2 \delta(E_n - E). \tag{1}$$

Here, $df(E,K)/dE$ represents GOSD. Ψ_0 and Ψ_n are the electronic wave functions of the initial and the final states, respectively, N is the anticipated number of electrons in the target, E_n is the excitation energy, and $\mathbf{r}_j$ is the position of the jth electron. In the limit $K \rightarrow 0$, the GOSD is identical to the optical oscillator strength density (OOSD). Within the nonrelativistic Born approximation, the GOSD is related to DDCS by the Bethe-Born formula (in atomic units)[1,2]

$$\frac{df(E,K)}{dE} = \frac{E}{2}\frac{p_0}{p_a} K^2 \frac{d^2\sigma}{dE d\Omega}. \tag{2}$$

Here, $df(E,K)/dE$ and $d^2\sigma/(dEd\Omega)$ represent the GOSD and DDCS, respectively. E and K are the excitation energy and momentum transfer, while p_0 and p_a are the incident and scattered electron momenta, respectively. According to its definition shown in Eq. (1), the absolute GOSD measured by angle-resolved electron-energy-loss spectrometer can be used to test the different theoretical methods as well as to assess accuracy of the wave functions, especially for the excited state's wave functions. Meanwhile, the generalized oscillator strengths (GOSs) or DCSs for different kinds of transitions versus angles show different behaviors; therefore, their shapes are helpful in determining correct spectral assignments [3,4]. Also as an important excitation method supplementary to photoabsorption, an electron impact method, such as electron-energy-loss spectroscopy, is a powerful tool to investigate the structures of atomic and molecular excitation states due to its nondipole excitation nature.

Up to now, most high-energy-resolution electron-energy-loss spectrometers have been employed to measure the optical oscillator strengths (OOSs) and GOSs below the first ionization threshold. The GOS measurements for superexcited states, i.e., excited states of molecules above the first ionization threshold such as high Rydberg states which are vibrationally (or/and rotationally), doubly-, or inner-shell excited, and non-Rydberg states [5–7], are fragmental due to the low cross sections and the difficulties in achieving required energy resolution. Meanwhile, there is increasing interest about the dynamics of superexcited states because superexcited states play an important role as reaction intermediates in a variety of collision processes such as electron-ion and ion-ion recombinations, Penning ionization, and electron attachment processes [5,6,8]. The three most commonly used methods to investigate the structure of superexcited states are the fluorescence spectroscopy emitted from neutral fragments, the photoelectron spectroscopy, and the photoion spectroscopy [7,9–11], each of which is related to one specific decay process of superexcited states. However, the spectra measured by angle-resolved electron-energy-loss spectroscopy include all possible decay processes for a specific state. As mentioned above, the momentum transfer dependence of different superexcited states is different; some superexcited states may stand out at large scattering angles. This is elucidated by recent work [12]. Therefore, angle-resolved electron-energy-loss spectroscopy with high energy

*Corresponding author. Email address: zpzhong@gscas.ac.cn

resolution may provide helpful information on the structure and nature of superexcited states. This is our main interest in this paper.

As one of the important atmospheric pollutants, NO plays a significant role in investigations of the natural environment such as the greenhouse effect, acid rain, ozone problem, etc., and it is also significant in development of lasers. In addition, the ground state of NO, i.e. $(1\sigma)^2(2\sigma)^2(3\sigma)^2(4\sigma)^2(1\pi)^4(5\sigma)^2(2\pi)^1$, can be referred to as a prototype molecule equivalent to an alkali atom in atomic system, so theoretical problems connected with the energy levels of the excited NO molecule are of great interest and importance. As for theoretical works, many studies have been carried out recently for the energy levels of excited NO, such as Refs. [13,14]. Among them, Zhong *et al.* [14] have calculated the photoabsorption spectrum of NO in the region of 9.3–22 eV by the multiple-scattering self-consistent-field (MSSCF or MS-X_α) method based on quantum defect theory (QDT), which is in general agreement with the available experimental data. Meanwhile, the energy levels of the Rydberg series resulting from the excitation of 1π, 5σ, or 4σ electron have been reported. With regard to experimental works, the energy levels of NO below the first ionization threshold have been studied extensively and well summarized by Huber and Herzberg [15]. As for the energy levels of NO above the first ionization threshold, Erman *et al.* [11] have analyzed and classified the Rydberg series converging to all known states of NO^+ below 24 eV, except the one converging to singlet ionization threshold of a 4σ electron. Recently, a number of peaks observed in the fluorescence spectrum in the energy region of 17.2–25.8 eV were assigned to "new" NO states since they showed a poor coincidence with the known NO Rydberg levels or other molecular states [9]. On the other hand, the electron energy loss spectra of NO below 55 eV were measured by Lee [16] in the scattering angle range of 0.5°–4° with high incident electron energy (25 keV) and low energy resolution (2.5 eV); a peak at 21.3 eV and a broad peak at 33 eV were observed at large momentum transfers, and Lee[16] suggested that the one at 21.3 eV is related to transitions to Rydberg states (including optically forbidden transitions) which converge to $^3\Pi$ or $^1\Pi$ of NO^+ or two electron transitions, and the one at 33 eV is related to the inner-valence transitions from $2\pi \leftarrow 3\sigma$. However, to the best of our knowledge no further electron impact works have been carried out for this energy region. In summary, although a number of experimental and theoretical studies of the excited energy levels of NO have been reported, some superexcited states of NO are still unidentified.

In the present work, we measured the electron energy loss spectra in the scattering angle range of 0°–8° with an interval of 2°, and absolute OOSD and DDCS have been determined. Some features above the first ionization threshold, which are too weak to be observed in the photoabsorption spectrum, stand out at large scattering angles. Based on the present experimental work and theoretical analysis, the present measured features as well as those unassigned ones in the fluorescence spectra are assigned.

II. EXPERIMENTAL METHOD

The angle-resolved electron-energy-loss spectrometer used in this work has been described in detail in Refs. [17–19]. Briefly, it consists of an electron gun, a hemispherical electrostatic monochromator made of aluminum, a rotable energy analyzer of the same type, an interaction chamber, a number of cylindrical electrostatic lenses, and a one-dimension position-sensitive detector for detecting the scattered electrons. All of these components are enclosed in four separate vacuum chambers made of stainless steel. The impact energy of the spectrometer can be varied from 1 to 5 keV. For the present experiment it was set at 2.5 keV and the energy resolution was about 100 meV. The background pressure in the vacuum chamber was 3×10^{-5} Pa and when the gas sample was entered, the pressure in the reaction chamber rose to 8×10^{-3} Pa. The true zero angle was calibrated by the symmetry of the angular distribution of the $A\ ^2\Sigma \leftarrow X\ ^2\Pi$ inelastic scattering signal around the geometry nominal zero. The angular resolution was about 0.8° (FWHM) at present.

The electron-energy-loss spectra of NO were measured in the scattering angle range of 0°–8° with an interval of 2°, and the energy calibration of the spectra was referred to the $5\sigma^{-1}(b\ ^3\Pi)3p\pi$ (13.82)[11]. Then, the spectrum measured at a mean angle of 0° was converted into relative OOSD spectrum by multiplying the Bethe-Born conversion factor of the spectrometer [17,20]. The spectra at other scattering angles were converted into relative GOSD spectra according to Eq. (2).

These relative GOSD spectra were made absolute by using the valence shell Bethe sum-rule [1,21]

$$S_{\mathrm{val}}(0) = N_{\mathrm{val}} + N_{\mathrm{PE}} = \int_{E'}^{\infty} \left(\frac{df}{dE}\right) dE, \tag{3}$$

where N_{val} is the total number of valence electrons in the target (11 for NO), N_{PE} is a small estimated correction (0.32 for NO) of the Pauli-excluded transitions from the K shells to the already occupied valence shell orbitals [22,23], and E' is the lowest excitation energy. In the limit $K \rightarrow 0$, the GOSD is identical to the OOSD which was obtained using the valence Thomas-Reiche-Kuhn (VTRK) sum rule [24]. In the sum-rule normalization procedure, the intensity of the relative OOSD or GOSD obtained at a particular scattering angle was first numerically integrated over a sampling energy loss range, i.e., up to 75 eV for 0°, 2°, and 4°, 93 eV for 6°, and 130 eV for 8°. The remaining intensity of the valence shell higher than the measured energy region for NO was estimated by integration of a fitted function $aE^{-1.5}+bE^{-2.5}+cE^{-3.5}$ from the limit of the measurements to infinity, where the empirical constants a, b, and c were determined by least–squares fitting to the experimental data in the energy loss range of 55–75 eV for 0°, 2°, and 4°, 73–93 eV for 6°, and 100–130 eV for 8°.

The overall percent error of the OOSD and DDCS obtained in the present work is no more than 20%, which mainly comes from the statistics of counts, the angular and energy position's determination, and the least–squares fitting procedure to obtain the intensity of the valence shell higher than the measured energy region. Note that the pressure effect is not included.

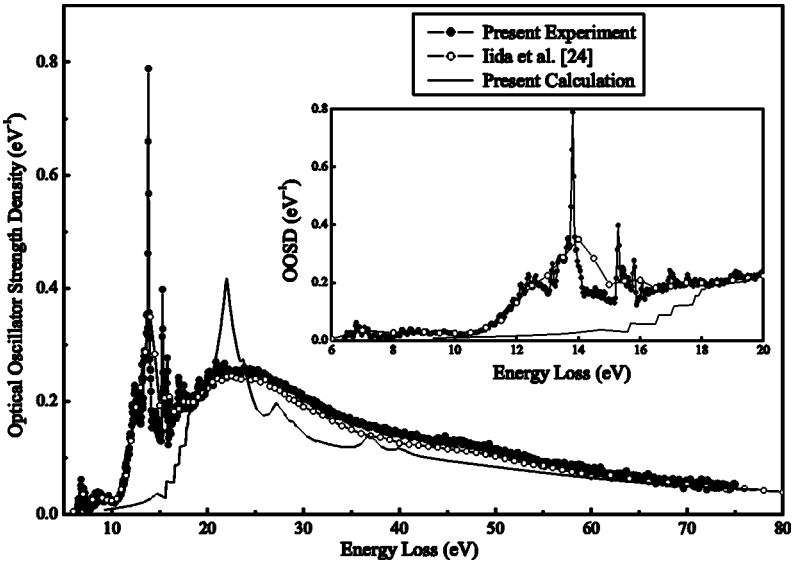

FIG. 1. Absolute OOSD of NO in the energy region of 5–80 eV. The inset shows the expanded spectra in the energy region 6–20 eV.

III. THEORETICAL METHOD

The MSSCF method was employed in this work. Briefly, based on a trial charge density of the molecule, a muffin-tin trial molecular potential V^{mol} with the symmetry of molecular point group was constructed. We can then calculate the occupied molecular orbitals (MOs), which serve to construct the charge density of the molecule and then a new trial molecular potential. With this process going on, self-consistent iterations were undertaken until a certain precision was met. A self-consistent-field (SCF) molecular potential $V_{\mathrm{scf}}^{\mathrm{mol}}$ was obtained and thereafter we can calculate all the MOs, including nondiffusive molecular orbitals (NMOs), Rydberg molecular orbitals (RMOs), and adjacent continuum molecular orbitals (CMOs), respectively. In our calculations, all the RMOs and CMOs were treated in a unified manner in the framework of QDT [25–30]. With the calculated wave functions, GOSD can be calculated [31] according to Eq. (1).

IV. RESULTS AND DISCUSSION

Figure 1 shows the experimental absolute OOSD spectra and the calculated photoionization OOSD. It can be seen that the present measured spectrum above 16 eV is in agreement with the previous experimental one [24] determined by the same method as ours but with higher impact energy of 8 keV and lower energy resolution of 1 eV. The discrepancy in the energy region below 16 eV (see the inset graph in Fig. 1) can be attributed to the different energy resolution. Meanwhile, the present calculated result generally agrees with the experimental data, except for the energy region of 9.2–18 eV (see the inset graph in Fig. 1). This discrepancy can be understood since our calculations are based on self-consistent calculations; thus, electron correlations (i.e., channel interactions) were ignored. In addition, the contributions from the autoionization Rydberg states were not included in our calculations.

Figure 2 exhibits the present absolute DDCS spectra at the scattering angles of 0°, 2°, 4°, 6°, and 8°. Note that with the increasing of K^2, the energy position of the very broad feature observed at the scattering angles of 6° and 8°, i.e., the Bethe ridge, moves to higher energy loss and the corresponding width becomes more diffuse. Such phenomena have also been observed in other molecules such as H_2O [32] and SF_6 [33]. Furthermore, some features marked as α and β stand out at large scattering angles. We will discuss these features in detail in the order of the excitation energy.

First, we will discuss the features in the energy region of 17.3–22 eV shown in Fig. 3, i.e., marked as α in Fig. 2. Here, R(A) and R(c) stand for the Rydberg series converging to $(5\sigma)^{-1}\,A\,{}^1\Pi$ and $(4\sigma)^{-1}\,c\,{}^3\Pi$ of NO^+, respectively. On the top of Fig. 3 the energy positions of R(A) and R(c) are taken from photoionization spectra [11], expect that of $R(c)ns\sigma$ are determined by this work according to the fluorescence spectrum of neutral atomic fragments [9]. Six ionization thresholds in this energy region, i.e. $(1\pi)^{-1}\,b'\,{}^3\Sigma^-$ (17.68 eV), $(1\pi)^{-1}\,A'\,{}^1\Sigma^+$ (17.91 eV), $(1\pi)^{-1}\,W\,{}^1\Delta$ (18.14 eV), $(1\pi)^{-1}\,{}^1\Sigma^-$ (19.84 eV), $(5\sigma)^{-1}\,A\,{}^1\Pi$ (18.33 eV), and $(4\sigma)^{-1}\,c\,{}^3\Pi$ (21.72 eV) are also indicated. As shown in Figs. 3(b) and 3(c), the Rydberg states related to

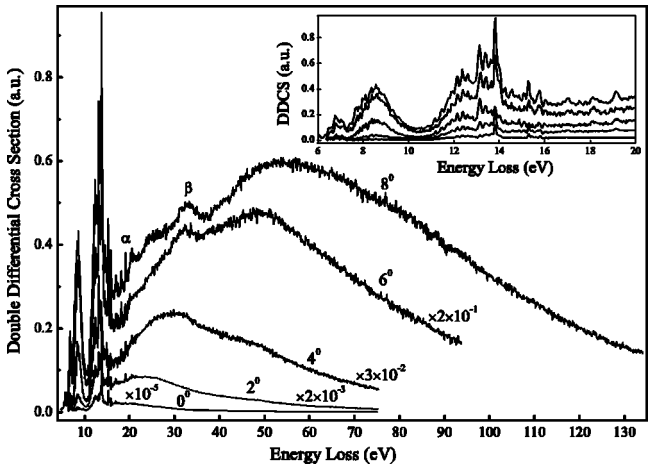

FIG. 2. DDCS of NO below 135 eV. α and β denote some features standing out at large scattering angle. The inset shows the expanded spectra in the energy region 6–20 eV.

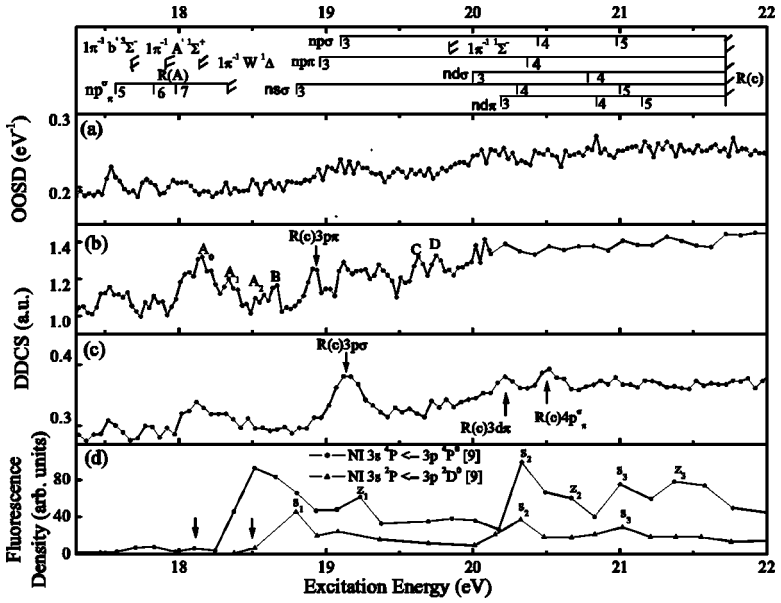

FIG. 3. Spectra of NO in the energy region of 17.3–22 eV: (a) OOSD; (b) and (c) DDCS measured at 6° and 8°, respectively; (d) fluorescence spectra [9]. On the top of OOSD spectrum the positions of the experimentally known NO Rydberg levels are indicated, except the $4\sigma^{-1}(c\ ^3\Pi)ns\sigma$ is assigned by this work. A_0, A_1, A_2, B, C, and D represent the features standing out at the scattering angle of 6°. The vertical arrows in (d) indicate the calculated thresholds for exciting the multiplet [9].

$R(c)np\sigma(n=3-4)$, $np\pi(n=3-4)$, and $3d\pi$, which are hardly observed in the photoabsorption spectrum due to the weak intensity [see Fig. 3(a)], stand out at the large scattering angle of 6° or 8°. Meanwhile, these superexcited states are not observed in the fluorescence spectra [see Fig. 3(d)], i.e., their primary decay paths are not neutral dissociation. As for the window-type series $(c\ ^3\Pi)ns\sigma$, it is difficult to estimate their presence in our experimental measurements. To the best of our knowledge $(c\ ^3\Pi)ns\sigma$ were only reported experimentally by photoionization spectra [11]. More specifically, the energy positions of $(4\sigma)^{-1}$ $(c\ ^3\Pi)4s\sigma$ and $(4\sigma)^{-1}(c\ ^3\Pi)5s\sigma$ are 20.26 and 20.90 eV, respectively, and $(4\sigma)^{-1}$ $(c\ ^3\Pi)3s\sigma$ is too weak to be observed. Note that the energy positions are a little lower than that of the peaks marked as S_1, S_2, and S_3 around 18.8, 20.3, and 21.0 eV, respectively, in the NI $3s\ ^2P \leftarrow 3p\ ^2D^0$ and NI $3s\ ^4P \leftarrow 3p\ ^4P^0$ fluorescence spectra. Since the structure of these excitation functions showed a poor coincidence with the known NO Rydberg levels taken from photoionization spectra [11], Ref. [9] suggested S_1, S_2, and S_3 may belong to "new" NO states. However, we suggest that S_1, S_2, and S_3 belong to $(4\sigma)^{-1}(c\ ^3\Pi)ns\sigma(n=3-5)$ Rydberg series. The reason is discussed as follows: the corresponding effective quantum numbers n^* of S_1, S_2, and S_3 are 2.16, 3.09, and 4.35, respectively, when the ionization threshold value is taken that of $(4\sigma)^{-1}c\ ^3\Pi$, i.e., 21.72 eV [15]. In addition, the intensity of the three peaks decreases as excitation energy increases, which is also similar to the behavior of a Rydberg series. Therefore, the assumption that the three peaks belong to a Rydberg series converging to $(4\sigma)^{-1}$ $c\ ^3\Pi$ is reasonable. The discrepancy between the data from photoionization spectrum and that from the fluorescence spectrum is understood as follows: the profile of a specific superexcited state may vary with different experimental methods, which would result in different accuracy in determining its energy position. In fact, S_1, S_2, and S_3 features are related to three peaks in the fluorescence spectrum, and corresponding energy position are undoubtedly determined by peak positions, while $(4\sigma)^{-1}(c\ ^3\Pi)ns\sigma(n=4-5)$ series is a window-type Rydberg series in the photoionization spectra [11] and their energy positions are determined by the minimum positions in Ref. [11]. However, the idealized resonance energy of an isolated atomic or molecular state above the first ionization threshold in the photoabsorption and photoionization spectra should be determined by a nonlinear parameter-fitting procedure according to the Beutle-Fano formula [34,35]

$$\sigma(\varepsilon) = \sigma_a[(q+\varepsilon)^2/(1+\varepsilon^2)] + \sigma_b. \tag{4}$$

Here, $\varepsilon=(E-E_r)/(\Gamma/2)$ indicates the departure of the excitation energy E from an idealized resonance energy E_r which pertains to a discrete autoionization state. Also, $\Gamma/2$ is the half linewidth of the autoionization resonance, q is a line profile index which represents the ratio of transition amplitude of the "modified" discrete state to that of the relevant continuum state, and a window-type state corresponds to q $\rightarrow 0$. Finally, $\sigma(\varepsilon)$ represents the absorption cross section at the excitation energy E, whereas σ_a and σ_b represent two portions of the cross section corresponding, respectively, to transitions to states of the continuum that interfere and do not interfere with the discrete autoionization state. Therefore, the errors of the energy positions of $(4\sigma)^{-1}(c\ ^3\Pi)ns\sigma$ reported by Ref. [11] should not be small. In addition, the weak window series $(4\sigma)^{-1}(c\ ^3\Pi)ns\sigma$ are overlapped with the strong series $(4\sigma)^{-1}(c\ ^3\Pi)nd\pi$ in the photoionization spectrum [11], so it is difficult to obtain the accurate energy positions of the weak window series. However, such difficulty can be avoided for the fluorescence spectroscopy method since the profile of a superexcited state in the fluorescence spectrum may not be a Beutle-Fano profile [see Fig. 3(d)] if it does not interact with the continuum. In such cases, the energy position of a superexcited state can be directly determined instead of being determined by a nonlinear parameter-fitting procedure according to Eq. (4). Furthermore, some structures stand out in the photoionization spectrum but vanish in the fluorescence spectrum such as the $(4\sigma)^{-1}(c\ ^3\Pi)nd\pi$; thus, overlapping is relieved or partially

relieved in the fluorescence spectrum. therefore, we recommend that the energy positions of the series $(4\sigma)^{-1}ns\sigma(n=3-5)$ are 18.8, 20.3, and 21.0 eV, respectively, taken from the fluorescence spectrum [see Fig. 3(d)].

Since the neutral dissociation probability of the series $(4\sigma)^{-1}(c\ ^3\Pi)ns\sigma(n=3-5)$ is large, the neutral dissociation probability of the series $(4\sigma)^{-1}(B\ ^1\Pi)ns\sigma(n=3-5)$ should not be small. However, to the best of our knowledge, no data for the energy positions of the series $(4\sigma)^{-1}(B\ ^3\Pi)ns\sigma(n=3-5)$ have been published and the ionization threshold of $(4\sigma)^{-1}B^1\Pi$ is still controversial. One assignment associates both the $c\ ^3\Pi$ and $B\ ^1\Pi$ states with the band at 21.7 eV [36]. The alternative assignment puts the $c\ ^3\Pi$ state at 21.7 eV and the $B\ ^1\Pi$ at 22.7 eV [37]. Note that the three unassigned features marked as Z_1, Z_2, and Z_3 in the NI $3s\ ^4P\leftarrow 3p\ ^4P^0$ fluorescence spectrum are around 19.2, 20.7, and 21.4 eV, respectively. Similarly, they may belong to a Rydberg series as discussed above. We suggest that the three features belong to the Rydberg series converging to $(4\sigma)^{-1}\ B\ ^1\Pi$; Therefore, the ionization threshold 22.1 eV of $(4\sigma)^{-1}B\ ^1\Pi$ is derived. That the assignment associates both the $c\ ^3\Pi$ and $B\ ^1\Pi$ states with the band at 21.7 eV [36] may be reasonable.

Now, let us discuss the features marked as A_0, A_1, A_2, B, C, and D which are overwhelmed in the photoabsorption spectrum [see Fig. 3(a)], and stand out at the large scattering angle of 6° or 8°. To the best of our knowledge, no assignments have been given for them. Note that the energy positions of the three prominent features A_0, A_1, and A_2 are around 18.1, 18.3, and 18.5 eV, respectively [see Fig. 3(b)], and the energy intervals among them are almost equal to 0.2 eV. Therefore, it is a reasonable suggestion that A_0, A_1, and A_2 may be ascribed to a vibrational progression of an electronic state. Furthermore, the electronic state cannot be a Rydberg state corresponding to the excitation of a 5σ, 1π, or 4σ electron; it may be a doubly excited state. The reason is discussed as follows: (1) Since the transition with $\Delta v'=0$, i.e, 0-0 transition, is dominant for the excitation of a 5σ electron due to the Franck-Condon principle (see the analysis in Ref. [14]), A_0, A_1, and A_2 cannot be the vibrational progression of a Rydberg state corresponding to the excitation of a 5σ electron; (2) Based on the calculated results by Zhong *et al.*[14] there is more than one Rydberg state resulting from the excitation of a 1π electron (see Table V in Ref. [14]) in the energy region of 17.3–22.0 eV, and the behaviors of GOS in a Rydberg series should be similar to each other. However, no other structures which are similar to A_0, A_1, and A_2 were observed; (3) The electronic state cannot be a Rydberg state resulting from the excitation of a 4σ electron based on the photoionization data taken from Ref. [11] (see the top of Fig. 3). Such a doubly excited state related to A_0, A_1, and A_2 may result from the transition of $2\pi^2\leftarrow 5\sigma^2$, $2\pi^2\leftarrow 4\sigma 5\sigma$, and/or $2\pi^2\leftarrow 1\pi 5\sigma$ based on the *ab initio* calculations [9]. On the other hand, the presence of A_0, A_1, and A_2 is also indicated in the NI $3s\ ^4P\leftarrow 3p\ ^4P^0$ fluorescence spectrum shown in Fig. 3(d). In fact, there is a broad peak around 18.5 eV. Considering the dissociation thresholds denoted by vertical arrows in Fig. 3(d), it is understandable that the features A_0 and A_1 are too weak to be observed in the NI $3s\ ^2P\leftarrow 3p\ ^2D^0$ fluorescence spectrum

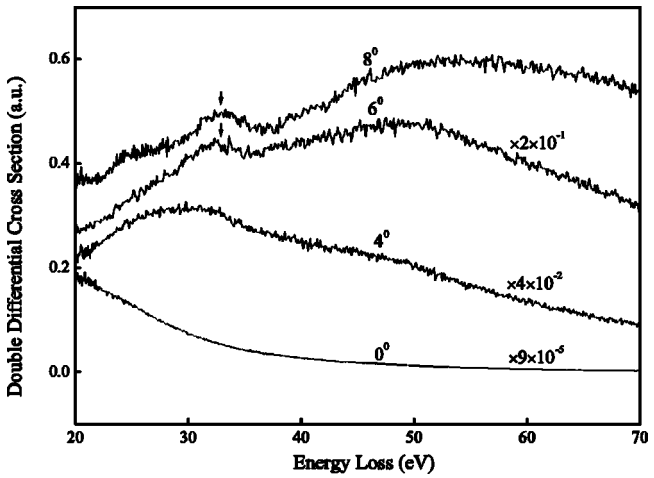

FIG. 4. DDCS of NO in the energy region of 20–72 eV.

[9]. The assignments for the features B, C, and D are an open question. Some of them may be ascribed to the Rydberg states resulting from the excitation of a 1π electron.

Finally, let us discuss the feature at 33 eV marked as β in Fig. 2. As shown in Fig. 4, the broad feature at 33 eV was not clearly observed until the scattering angle increases to $6°(K^2\sim 2$ a.u.). This feature was also observed in Ref. [16] at $K^2\geqslant 2.1$ a.u.$(\theta\geqslant 2.0°)$. Lee [16] suggested that the feature may be assigned to the transition of $2\pi\leftarrow 3\sigma$, and the existence of a minimum followed by a maximum in the GOS of the feature results in the phenomenon, i.e., the feature stands out at large momentum transfers. In order to elucidate the phenomenon, we calculated the excitation energy of the transition of $2\pi\leftarrow 3\sigma$ and its GOS curve versus K^2 based on the MSSCF method as shown in Fig. 5. The calculated energy position is 32.4 eV, which is close to the observed energy position 33 eV. It can be seen from Fig. 5 that there is only a maximum in the region of $K^2=0.8-3.6$ a.u. (i.e., the scattering angle range of $4°-8°$ under the present experimental conditions), which is in agreement with our observation (see Fig. 4). Therefore, the broad feature at 33 eV is assigned to the transition of $2\pi\leftarrow 3\sigma$ based on our calculations.

V. CONCLUSION

The electron-energy-loss spectra of NO have been measured in the scattering angle range of $0°-8°$ with an interval

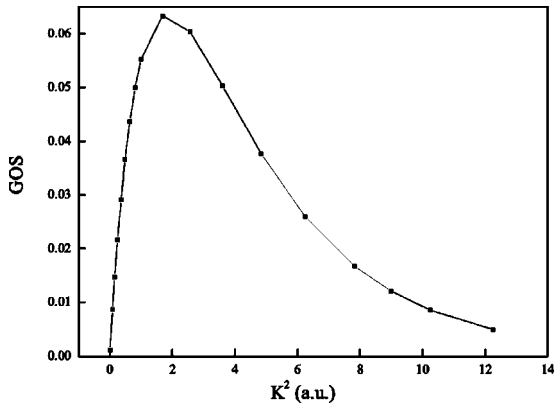

FIG. 5. The calculated GOS for $2\pi\leftarrow 3\sigma$ transition of NO.

of 2°; then, absolute OOSD and DDCS have been obtained (see Figs. 1 and 2). Interestingly, some superexcited states stand out at large scattering angles (see Figs. 2–4). Based on the present experimental work and theoretical analysis, most of the measured features and the ones in the fluorescence spectra [9] are assigned. Therefore, the energy levels of $4\sigma^{-1}(c\ ^3\Pi)ns\sigma(n=3-5)$, $4\sigma^{-1}(B\ ^1\Pi)ns\sigma(n=3-5)$, a vibrational resolved doubly excited state and the inner–valence transition $2\pi\leftarrow 3\sigma$ are determined. More specifically (1) the features marked as S_1, S_2, and S_3 in Fig. 3(d) taken from the fluorescence spectra [9] around 18.8, 20.3, and 21.0 eV, respectively, are ascribed to the $(4\sigma)^{-1}(c\ ^3\Pi)ns\sigma(n=3-5)$ Rydberg states. The discrepancy between the data from photoionization spectrum and that from the fluorescence spectrum is explained, and the energy positions of the $(4\sigma)^{-1}(c\ ^3\Pi)ns\sigma(n=3-5)$ Rydberg states taken from the fluorescence spectra [9] are recommended. (2) The features marked as Z_1, Z_2, and Z_3 in Fig. 3(d) taken from the fluorescence spectrum [9] around 19.2, 20.7, and 21.4 eV, respectively, are ascribed to the $(4\sigma)^{-1}(B\ ^1\Pi)ns\sigma(n=3-5)$ Rydberg states. Thus, the ionization threshold 22.1 eV of $(4\sigma)^{-1}B\ ^1\Pi$ is estimated. (3) The three features marked as A_0, A_1, and A_2 [see Fig. 3(b)] around 18.1, 18.3, and 18.5 eV, respectively, may belong to a vibrational progression of a doubly excited state. The doubly excited state may result from the transition of $2\pi^2\leftarrow 5\sigma^2$, $2\pi^2\leftarrow 4\sigma 5\sigma$, and/or $2\pi^2\leftarrow 1\pi 5\sigma$ based on the *ab initio* calculations [9]. (4) The feature around 33 eV is ascribed to the transition of $2\pi\leftarrow 3\sigma$ based on our calculations.

As elucidated in this paper, angle-resolved electron-energy-loss spectroscopy includes all possible decay processes for a specific state, and some superexcited states may stand out at large scattering angles. Therefore, it is an important method supplementary to the three most commonly used methods to investigate the structure of superexcited states, i.e., the fluorescence spectroscopy of neutral atomic fragments, the photoelectron spectroscopy, and the photoion spectroscopy, each of which is related to one specific decay process of superexcited states.

Support of this work by the National Nature Science Foundation of China (10134010, 10004010) and the Youth Foundation of the University of Science and Technology of China is gratefully acknowledged.

[1] M. Inokuti, Rev. Mod. Phys. **43**, 297 (1971).
[2] H. Bethe, Ann. Phys. (Leipzig) **5**, 325 (1930); Z. Phys. **76**, 293 (1930).
[3] R. A. Bonham, *Electron Spectroscopy: Theory, Techniques and Applications*, edited by C. R. Brundle and A. D. Baker (Academic, New York, 1979), Vol. 3, p. 127.
[4] E. N. Lassettre and A. Skerbele, *Methods of Experimental Physics*, edited by D. Williams (Academic, New York, 1974), Vol. 3, Pt. B, p. 868.
[5] R. L. Platzman, Radiat. Res. **17**, 419 (1962).
[6] R. L. Platzman, Vortex **23**, 372 (1962).
[7] Y. Hatano, Phys. Rep. **313**, 109 (1999).
[8] Y. Hatano, Radiat. Phys. Chem. **67**, 187 (2003).
[9] E. Melero García, J. Álvarez Ruiz, P. Erman, A. Kivimäki, E. Rachlew-Källne, J. Rius i Riu, M. Stankiewicz, and L. Veseth, Chem. Phys. **293**, 65 (2003).
[10] A. Ehresmann, H. Liebel, M. Von Kröger, and H. Schmoranzer, J. Phys. B **34**, 3119 (2001).
[11] P. Erman, A. Karawajczyk, E. Rachlew-Källne, and C. Strömholm, J. Chem. Phys. **102**, 3064 (1995).
[12] Z. P. Zhong, X. Y. Han, W. H. Zhang, and J. M. Li, Chin. Phys. Lett. **21**, 279 (2004).
[13] M. R. Hermann, C. W. Bauschlicher, Jr., W. M. Huo, S. R. Langhoff, and P. W. Langhoff, Chem. Phys. **109**, 1 (1986).
[14] Z. P. Zhong, W. H. Zhang, and J. M. Li, J. Chem. Phys. **113**, 136 (2000).
[15] P. Huber and G. Herzberg, *Molecular Spectra and Molecular Structure* (Van Nostrand, Princeton, 1979), Vol. 4.
[16] J. S. Lee, J. Chem. Phys. **67**, 3998 (1977).
[17] S. L. Wu, Z. P. Zhong, R. F. Feng, S. L. Xing, B. X. Yang, and K. Z. Xu, Phys. Rev. A **51**, 4494 (1995).
[18] K. Z. Xu, R. F. Feng, S. L. Wu, Q. Ji, X. J. Zhang, Z. P. Zhong, and Y. Zheng, Phys. Rev. A **53**, 3081 (1996).
[19] X. J. Liu, L L. F. Zhu, X. M. Jiang, Z. S. Yuan, B. Cai, X. J. Chen, and K. Z. Xu, Rev. Sci. Instrum. **72** 3357 (2001).
[20] W. F. Chan, G. Cooper, and C. E. Brion, Phys. Rev. A **44**, 186 (1991).
[21] T. N. Olney, N. M. Cann, G. Cooper, and C. E. Brion, Chem. Phys. **223**, 59 (1997).
[22] J. A. Wheeler and J. A. Bearden, Phys. Rev. **46**, 755 (1934).
[23] J. L. Dehmer, M. Inokuti, and R. P. Saxon, Phys. Rev. A **12**, 102 (1975).
[24] Y. Iida, F. Carnovale, S. Daviel, and C. E. Brion, Chem. Phys. **105**, 211 (1986).
[25] X. C. Pan, X. L. Liang, and J. M. Li, Acta Phys. Sin. **36**, 426 (1987) (in Chinese).
[26] L. Liu and J. M. Li, J. Phys. B **24**, 1893 (1991).
[27] K. H. Sze, C. E. Brion, X. M. Tong, and J. M. Li, Chem. Phys. **115**, 433 (1987).
[28] X. M. Tong, J. M. Li, K. H. Sze, and C. E. Brion, in 14th International Conference on X-ray Inner-shell Processes, Paris, France, 1987 (unpublished).
[29] X. M. Tong and J. M. Li, J. Phys. B **22**, 1531 (1989).
[30] X. M. Tong and J. M. Li, in *Sixteenth International Conference on the Physics of Electronic and Atomic Collisions*, edited by A. Dalgarno, R. S. Freund, M. S. Lubell, and T. B. Lucatorto, AIP Conf. Proc. No. 205 (AIP, New York, 1990).
[31] X. Y. Han, W. H. Zhang, and J. M. Li (unpublished).
[32] M. Dingfelder and M. Inokuti, Radiat. Environ. Biophys. **38**, 93 (1999).
[33] C. C. Turci, J. T. Francis, T. Tyliszczak, G. G. de Souza, and A. P. Hitchcock, Phys. Rev. A **52**, 4678 (1995).
[34] U. Fano, Phys. Rev. **124**, 1866 (1961).
[35] U. Fano and J. W. Cooper, Phys. Rev. **153**, 1364 (1965).
[36] O. Edqvist, L. Åsbrink, and E. Lindholm, Z. Naturforsch. A **26a**, 1407 (1971).
[37] H. Lefebvre-Brion, Chem. Phys. Lett. **9**, 463 (1971).